(11) Klein, J.; Luckham, P. F. *Macromolecules* **1984**, *17*, 1048.
(12) Klein, J.; Luckham P. F. *Nature (London)* **1984**, *308*, 836.
(13) Luckham, P. F.; Klein, J. *Macromolecules* **1985**, *18*, 721.
(14) Brandrup, J.; Immergut, E. H., Eds. *Polymer Handbook*; Wiley: New York, 1975.
(15) de Gennes, P.-G. *Macromolecules* **1981**, *14*, 1637; **1982**, *15*, 429.
(16) de Gennes, P.-G. *Scaling Concepts in Polymer Ppysics*; Cornell University Press: Ithaca, NY, 1979.
(17) The existence of anomalous scaling exponents very near the surface should not influence the present discussion: see, for example: de Gennes, P.-G.; Pincus, P. *J. Phys. Lett.* **1984**, *45*, L 953 and also Binder, K.; Kremer, K. *NATO Adv. Study Inst. Scaling in Disordered Systems*, in press.
(18) Flory, P. J. *Principles of Polymer Chemistry*; Cornell University Press: Ithaca, NY, 1953.
(19) Strictly speaking one should consider the effective "span" of the polymer: this is comparable with or slightly larger than R_0 in the unperturbed state—see: Rubin, R. J.; Mazur, J.; Weiss, G. H. *Pure Appl. Chem.* **1976**, *46*, 143. As this is an average value, in practice some segments will be extended considerably beyond this.
(20) Scheutjens, J. M. H. M.; Fleer, G. J. *Adv. Colloid Interface Sci.* **1982**, *16*, 341, 360; *Macromolecules* **1985**, *18*, 1882.
(21) Almog, Y.; Klein, J. *J. Colloid Interface Sci.* **1985**, *106*, 33.
(22) Israelachvili, J. N.; Tirrell, M.; Klein, J.; Almog, Y. *Macromolecules* **1984**, *17*, 204.

Craze Fibril Stability and Breakdown in Polystyrene

Arnold C.-M. Yang and Edward J. Kramer*

Department of Materials Science and Engineering and the Materials Science Center, Cornell University, Ithaca, New York 14853

Chia C. Kuo and S. Leigh Phoenix

Department of Mechanical and Aerospace Engineering and the Materials Science Center, Cornell University, Ithaca, New York 14853. *Received January 6, 1986*

ABSTRACT: Craze fibril stability of polymer glasses can be characterized by measuring the median strain (craze fibril stability) at the onset of craze fibril breakdown in thin films under a constant low strain rate. Monodisperse polystyrenes (PS's) of molecular weight M = 37 000–20 000 000 were used. A strong increase in craze fibril stability was found as M increased from 50 000 to 200 000. The increase occurred over the same range as the increase in macroscopic fracture toughness of PS. Voids were observed to always nucleate at the bulk–craze interface and never in the craze midrib. Higher strain rates reduced the craze fibril stability. Foreign particle inclusions, e.g., dust, in specimens can significantly decrease the fibril stability from its intrinsic (clean) value. Even in the presence of such particles, however, the M dependence of fibril stability is qualitatively similar to that of crazes in "dust-free" films. The fibril breakdown statistics can be investigated by examining simultaneously the failure events in a large number of independent film specimens. The statistics of craze fibril breakdown are found to follow a Weibull distribution. Two parameters may be extracted by fitting this distribution to the breakdown data: (1) a Weibull scale parameter ϵ_W, which is a measure of craze fibril stability, and (2) a Weibull modulus ρ, which is a measure of variability, that is, the breadth of the distribution of fibril stability (high ρ's produce narrow distributions and vice versa). The Weibull distribution in a weakest-link setting can be used to predict the effect of sample size on the probability of craze fibril breakdown somewhere in the sample. A microscopic statistical model in which craze fibrils fail by random disentanglement of molecular strands at the craze–bulk interface is developed. The experimental observations are in good agreement with the predictions of the model.

Introduction

The brittle fracture commonly observed in many glassy polymers under tension can be traced to the formation and breakdown of crazes, localized microdeformation zones composed of many aligned fibrils.[1-4] The fibrils are drawn from a narrow layer of strain-softened polymer on the bulk polymer–craze interfaces. As initially drawn the fibrils are usually strongly load-bearing and bridge between these two interfaces. It is observed, however, that craze fibrils can break down to form large voids which are the first stage in catastrophic fracture.[5-7] Thus the mechanisms of fibril breakdown are of crucial importance in the study of the fracture properties of these matterials.

Previous work on craze fibril stability has focused primarily on theoretical description and indirect measurements in poly(methyl methacrylate) (PMMA). Verheulpen-Heymans[8] explored theoretically craze failure in PMMA by assuming that fibrils fail by disentanglement of chains in the midrib, the layer of fibrils in the center of the craze. This fibrillar material forms just behind the craze tip and thus is the oldest region of the craze. Schirrer and co-workers[9,10] have inferred a "disentanglement time" involved in such failure of craze fibrils in PMMA by observing the craze–crack optical thickness profiles by interference optical microscopy. However, to understand the craze fibril breakdown mechanisms we first must be able to measure the onset of such breakdown directly. In this paper, we introduce a simple test from which the fibril stability and the fibril breakdown statistics can be determined. This test will enable us to explore the mechanisms of fibril breakdown and the molecular factors controlling the craze fibril stability.

Experimental Procedures

Thin films of monodisperse polystyrene (PS) ($M_w/M_n < 1.3$) were prepared from polymer of molecular weight M = 37 000, 50 000, 110 000, 233 000, 390 000, 900 000, 1 800 000, and 20 000 000 purchased from Pressure Chemical Co. The PS was dissolved in toluene, and uniform thin films were formed by drawing glass microscope slides from the solution at a constant speed. The film thickness was measured with a Zeiss interference microscope and was held constant at 0.4 μm. After the solution had escaped, the film was floated off the slide onto the surface of a water bath, and subsequently picked up on a ductile copper grid. The bars of this grid had previously been coated with a thin layer of PS by dipping the copper grid into a PS solution. A brief exposure to toluene vapor removed any slack in the film and served to bond the film to the copper grid.[11] This process enables each of the

0024-9297/86/2219-2010$01.50/0

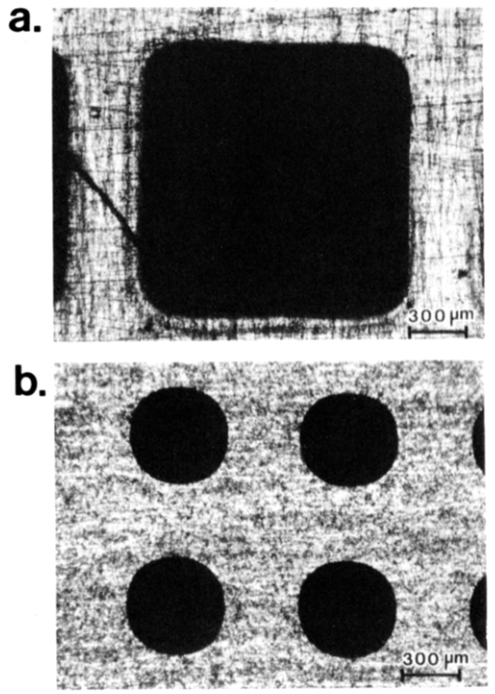

Figure 1. Optical micrographs of annealed copper grids which were used for supporting the PS films: (a) standard grid; (b) smaller grid with an area about 9 times smaller than (a).

grid bars to transfer strain to the supported PS film when the grid was deformed. To remove any possible residual solvent, specimens were stored under vacuum at room temperature for 35 h before testing.

The role of the copper grid was to subdivide the PS film into a large number (~40) of independent film squares for the purposes of studying the breakdown statistics. Each film square was approximately 1 mm × 1 mm. Copper grids with a smaller mesh size were also used to check for a size effect on fibril breakdown. The area of each film square was about 9 times smaller for this grid than for the standard grid. Optical micrographs of the two grids are shown in Figure 1.

The grids were deformed in tension by a strain frame coupled to a motor drive by which the strain rate could be controlled. As the film was strained, an optical microscope was used to monitor a sequence of three events, craze initiation, local craze fibril breakdown, and catastrophic fracture. Figure 2 displays mimcrographs showing craze initiation, fibril breakdown, and catastrophic fracture in a film square. Crazes usually initiated at the grid bars and across most of the film squares. A void resulting from local fibril breakdown was observed by reflected light microscopy as a growing black spot within the craze. The first observation of such a black spot within a craze in the film square was used as the criterion for fibril breakdown. Obviously this criterion cannot quite detect fibril breakdown at the earliest stage because of the low magnification employed. It is, however, a reliable and consistent criterion and easily detects differences between different polymers. Our criterion for catastrophic fracture was the growth of a crack longer than one half the side of a grid square anywhere within it.

For some experiments films were drawn from solutions which had been filtered to reduce the dust particle content. Dust particles were removed by passing the solution through a porous ceramic filter with an average pore size of 10 or 20 μm. Two groups of filtered specimens were made. "Clean" samples were cast from the solution filtered with the 20-μm filter and prepared under an ordinary clean hood. "Ultraclean" samples were cast from the filtered solutions (10-μm pore size) and prepared under the class 10 dust-free clean hood in the clean room of the National Research and Resource Facility for Submicron Structure (NRRFSS), Knight Laboratory, Cornell University. The filtering process and thin-film casting were also done in the class 10 clean hood.

An Ostwald viscometer was used to check for possible molecular weight degradation during filtering. The specific viscosity η_{sp} of the PS solutions before and after the filtering was measured inside

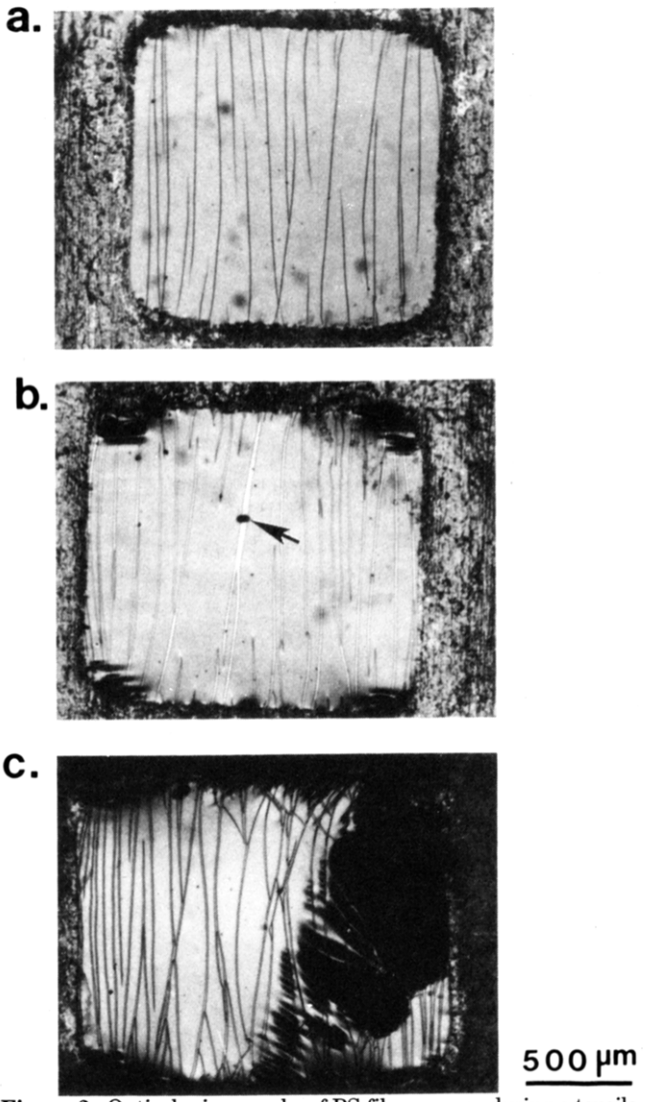

Figure 2. Optical micrographs of PS film squares during a tensile test illustrating (a) craze initiation, (b) local fibril breakdown (marked with arrow), and (c) catastrophic fracture. Tensile stress is in the horizontal direction.

a water bath maintained at 21 °C. Viscosity-average molecular weights M_v were calculated from the Mark–Houwink equation, $[\eta] = KM^{\alpha}$, using $K = 1.0 \times 10^{-5}$ m^3/kg and $\alpha = 0.73$. No molecular weight degradation was found from the filtering process and thus the narrow distribution in molecular weight was preserved in the films produced from the filtered solutions.

Experimental Results

Effects of Molecular Weight and Dust Particles. The cumulative number fractions of the film squares which had undergone craze initiation, p_c, local fibril breakdown, p_b, and catastrophic fracture, p_f, respectively could be monitored at various strains during the tensile test. Figure 3 shows p_c, p_b, and p_f as functions of strain for one test. Since the test was interrupted for the observation period, efforts were made to keep the observation time as brief as possible, typically 3–5 min. A typical test might last 18 h and requires approximately 12 such observations. Before each test, film squares which contained large dust particles or which were badly bonded were removed from consideration.

The full curve p_b in Figure 3 provides useful information on the fibril breakdown statistics and will be explored later with a Weibull model. For the present we report the optical microscopy data quantitatively as the median strains ϵ_c, ϵ_b, and ϵ_f (defined as $p_c(\epsilon_c) = 0.5$, $p_b(\epsilon_b) = 0.5$,

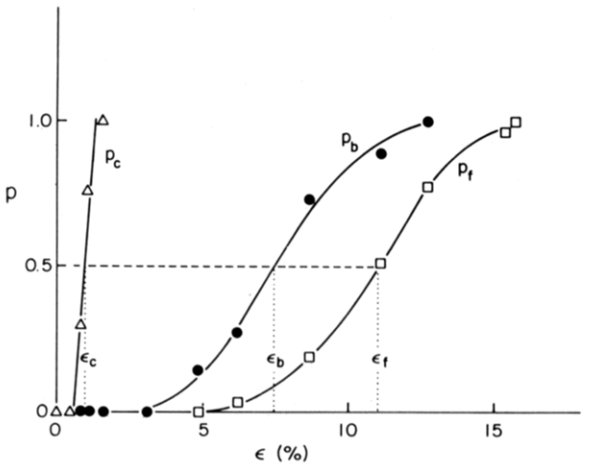

Figure 3. Cumulative number fraction of film squares (a) that have crazed (p_c (△)), (b) where craze fibrils have broken down (p_b (●)), and (c) where crazes have fractured (p_f (□)) plotted as a function of tensile strain (M = 900 000, unfiltered, strain rate = 3×10^{-6} s^{-1}).

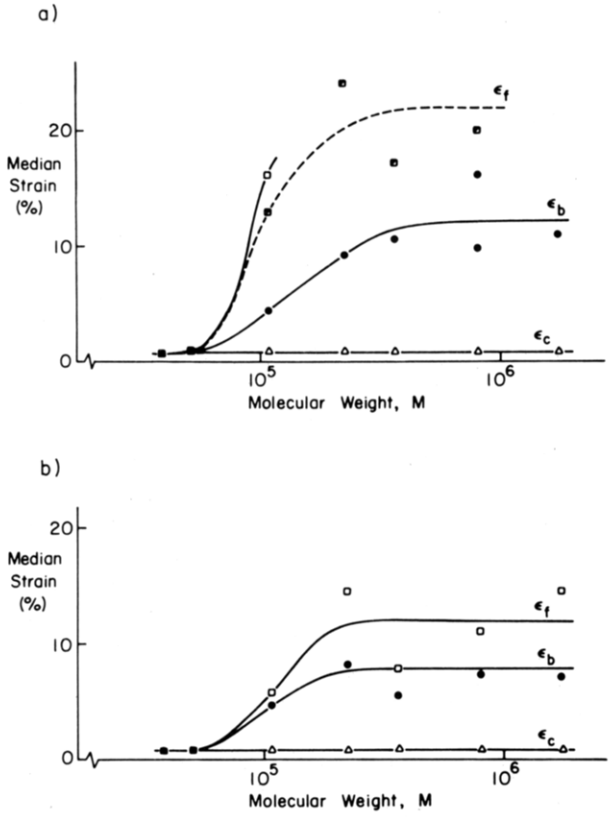

Figure 4. Median strains for crazing ϵ_c (△), fibril breakdown ϵ_b (●), and catastrophic fracture ϵ_f (□) vs. molecular weight M for the unfiltered specimens: (a) strain rate = 5×10^{-7} s^{-1}; (b) strain rate = 3×10^{-6} s^{-1}. (◪) Catastrophic fracture at $p_f = 0.25$.

$p_f(\epsilon_f) = 0.5$) for crazing, fibril breakdown, and catastrophic fracture, respectively, as shown in Figure 3.

The three median strains of the unfiltered specimens are plotted vs. M in Figure 4 for the two low strain rates, 5×10^{-7} and 3×10^{-6} s^{-1}, at room temperature. Because the solutions were not filtered, dust particle inclusions were present in these specimens. The median crazing strain ϵ_c is constant with molecular weight M within experimental error; the values are approximately 0.9% at 5×10^{-7} s^{-1} and 0.7% at 3×10^{-6} s^{-1}. On the other hand, for craze fibril breakdown and catastrophic fracture, the quantities ϵ_b and ϵ_f show a sharp increase with M in the region 50 000–200 000 and level off thereafter. During the test we did not notice any stable craze formation in the 37 000 and 50 000 molecular weight PS's even using these low strain rates. Once crazes formed they broke down immediately to form voids, and crack propagation occurred almost immediately thereafter. For $M \geq 110\,000$, stable crazes were always observed. The crazes in these samples can be grown as wide as 30 μm so that the fibril breakdown can be clearly examined, as illustrated Figures 2 and 5.

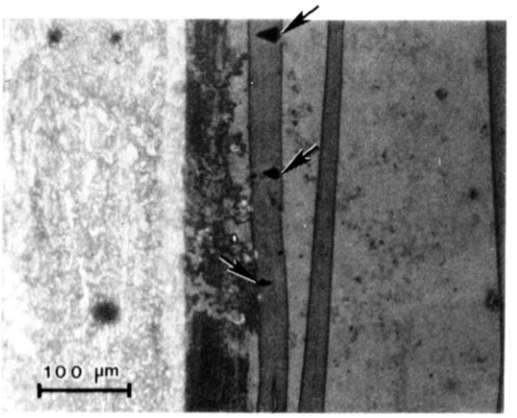

Figure 5. Optical micrograph showing typical craze fibril breakdowns (marked with arrows) nucleated from the craze–bulk interface.

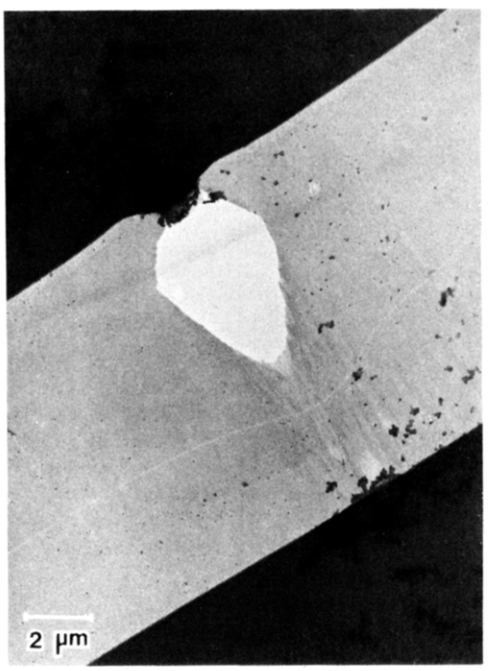

Figure 6. TEM micrograph of craze fibril breakdown at a dust particle inclusion in PS.

An increase in strain rate leads to a significant reduction in ϵ_b and ϵ_f in Figure 4. The median strain to fracture ϵ_f was not measurable for some of the high molecular weight films at the slower strain rate because the copper grid itself would fail first.

Both optical and transmission electron microscopy revealed that the fibril breakdown in PS crazes always initiated at the bulk polymer–craze interface. Breakdown begins by formation of a pear-drop-shaped cavity, attached to the interface, as shown in Figure 5. This behavior for crazes in PS is unlike that for crazes in PMMA, which are reported to fail at the midrib.[9,10] Closer examination was carried on under TEM. The samples were cut from the deformed copper grid at strains where $p_b \approx 0.5$. TEM observation revealed that craze fibrils broke down preferentially at the dust particle inclusions (Figure 6).

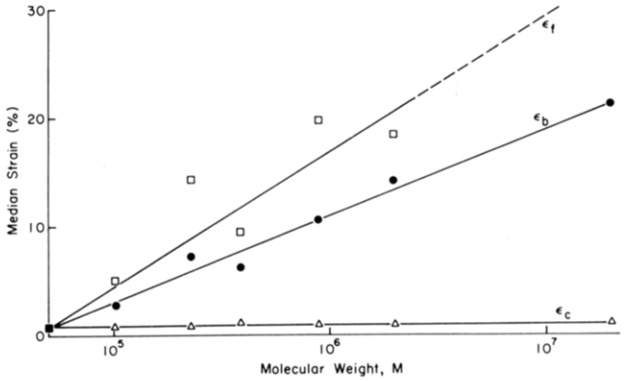

Figure 7. Median strains for crazing ϵ_c (△), fibril breakdown ϵ_b (●), and catastrophic fracture ϵ_f (□) vs. molecular weight for "clean" samples. Strain rate of test was 3×10^{-6} s^{-1}.

However, with, or without, the presence of the dust inclusions, these fibril breakdowns always occurred near the craze–bulk interface, confirming the optical microscopy observation.

The inclusions were randomly distributed, had random shapes, and were hard to classify and correlate with their effectiveness for craze fibril breakdown. From our limited survey using TEM, a trend of earlier fibril breakdown with increasing inclusion size was observed for the hard inclusions, which typically had less associated fibrillation. Generally when large inclusions were encountered, the fibrillation stopped, and the drawn fibrils underwent breakdown to form a cavity at the interface, as shown in Figure 6. For smaller inclusions, the craze-widening process often could continue. For small inclusions, in rare cases, a breakdown cavity could nucleate after the craze–bulk interface had advanced a short distance, creating a cavity some distance away from the interface. The cases were the only exceptions to the observation that the breakdown voids are always connected to the craze–bulk interface. At the strain rates used here, the transition from large-inclusion to small-inclusion behavior occurred at an inclusion diameter of about 0.1–0.5 μm.

In the unfiltered specimens, voids from fibril breakdown occasionally were found at the craze–bulk interfaces without the presence of any identifiable inclusions. These so-called "inherent weak spots" are believed to represent the intrinsic fibril breakdown.

For the "clean" PS specimens the craze breakdown and fracture strain ϵ_b and ϵ_f increased significantly over that of the unfiltered PS specimens for molecular weights $M \geq 110\,000$. The low molecular weight PS's of 50 000 and 37 000 nevertheless were still very fragile and failed approximately at the same strains for both sets of specimens. The higher strain rate 3×10^{-6} s^{-1} was used. Figure 7 shows plots of the median strains ϵ_c, ϵ_b, and ϵ_f vs. molecular weight of the "clean" specimens. Again ϵ_c is constant with the molecular weight, while ϵ_b and ϵ_f increase roughly linearly with the logarithm of M, instead of leveling off at high M as they do for the unfiltered PS specimens. When the breakdown sites were examined under TEM, however, we found that more than 50% of the fibril breakdown occurred at inclusions. Even in the "clean" PS specimens the dust particle inclusions still play an important role in the fibril breakdown. Intrinsic fibril breakdown, however, was much more frequently observed.

When virtually all the dust particles were removed in the "ultraclean" PS specimens, the craze fibril stability increased still further, except for the low molecular weights of 37 000 and 50 000. In fact, all median catastrophic fracture strains ϵ_f, and for some high molecular weight

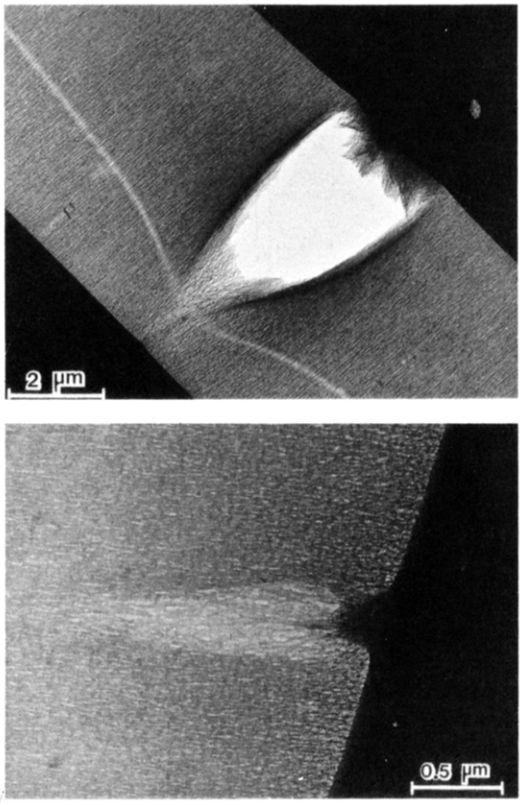

Figure 8. TEM micrograph of fibril breakdowns in the "ultraclean" specimens where no dust particle inclusions were present.

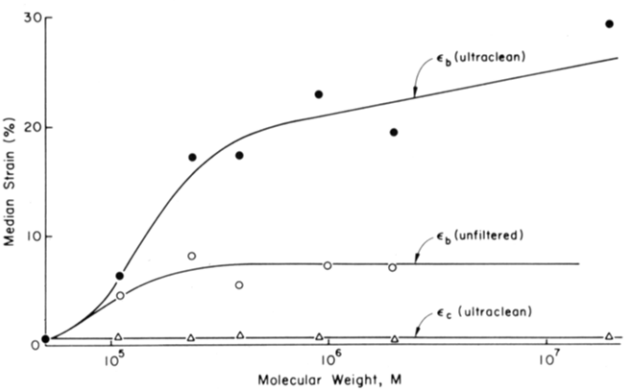

Figure 9. Median strains for crazing ϵ_c (△) and fibril breakdown ϵ_b (●) in the "ultraclean" samples vs. molecular weight. Also shown are the ϵ_b's (○) for the unfiltered samples.

samples, the median breakdown strains ϵ_b were too high to be measured. TEM observation showed that most of the fibril breakdowns were not associated with dust particles but were instead intrinsic craze fibril breakdowns. Figure 8 shows typical TEM micrographs of intrinsic breakdown sites. Plots of the median strains ϵ_c and ϵ_b vs. molecular weight for the "ultraclean" PS specimens are shown in Figure 9. The crazing strain ϵ_c is still independent of molecular weight, while fibril breakdown strain ϵ_b manifests a sharp increase between $M = 50\,000$ and 200 000 and then increases approximately linearly with the logarithm of molecular weight. The values of ϵ_b for the molecular weights 900 000 and 20 000 000 were obtained by extrapolating the measured data (low p vs. ϵ) to $p_b = 0.5$ using a Weibull distribution, since, as we will present in the next section, craze fibril breakdown follows Weibull statistics.

Craze Breakdown Statistics. In Appendix 1 we demonstrate that a reasonable form for the probability of

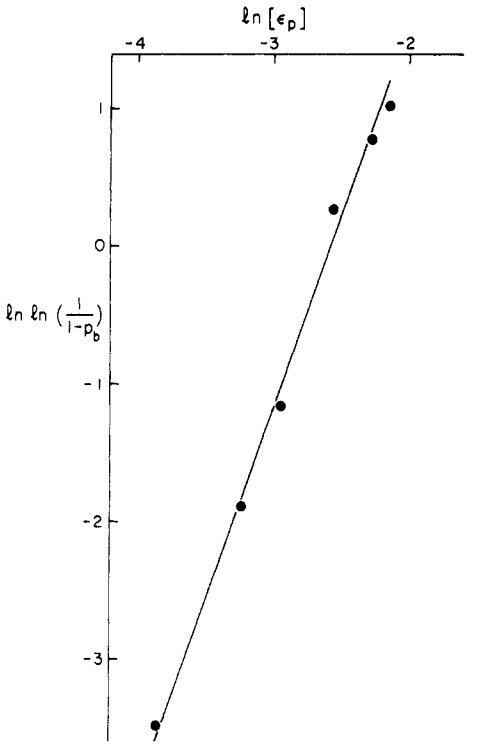

Figure 10. Typical Weibull plot, ln [ln(1/(1 − p_b))], vs. ln ϵ_p for craze fibril breakdown in PS. (M_w = 900 000, unfiltered, strain rate = 3 × 10^{-6} s^{-1}.)

craze fibril breakdown $\mathbf{p}(\epsilon_p)$ at a plastic strain ϵ_p is the Weibull distribution[12,13]

$$\mathbf{p}(\epsilon_p) = 1 - \exp[-(V_0/V_b)(\epsilon_p/\epsilon_W)^\rho] \quad (1)$$

where ρ is the Weibull modulus or shape parameter, ϵ_W is the Weibull scale parameter, V_0 is the initial grid square volume, and V_b is a volume in which one fibril breakdown will be encountered at a reference stress of σ_b.

By taking logarithms twice, one can write eq 1 in the form

$$\ln \{\ln [1/(1 - \mathbf{p})]\} = \rho \ln (\epsilon_p) - \rho \ln (\epsilon_W) + \ln (V_0/V_b) \quad (2)$$

The Weibull scale parameter ϵ_W and modulus ρ can be determined from the y intercept and the slope, respectively, of a plot of ln {ln [1/(1 − **p**)]} vs. ln (ϵ_p), the so-called Weibull plot. (For the large film squares we chose V_0/V_b = 1; thus for the small ones V_0/V_b = $^1/_9$.)

Next consider N_0 statistically independent film squares in a grid. An experimental measure of the probability of fibril breakdown $\mathbf{p}(\epsilon_p)$ at plastic strain ϵ_p is in fact $p_b(\epsilon)$, the cumulative number fraction of the film squares undergoing fibril breakdown at the grid strain $\epsilon = (\epsilon_c + \epsilon_p)$. The quantities ρ and ϵ_W therefore could be extracted from a replot of a curve (e.g., Figure 3) of p_b vs. ϵ. A typical Weibull plot for craze breakdown in PS obtained in this way is shown in Figure 10. The line is a least-squares fit to the experimental data. It clearly indicates that craze fibril breakdown is well modeled by a Weibull distribution.

In the three groups of samples, unfiltered, clean, and ultraclean PS films, the Weibull scale parameter ϵ_W increases with molecular weight in a manner which closely parallels the increases of the median strain for fibril breakdown ϵ_b in the same films. Figure 11 shows ϵ_W vs. M. It implies that ϵ_W can be used as an indicator of craze fibril stability. On the other hand, the behavior of the Weibull modulus ρ is more complicated. In practical terms a higher ρ leads to a steeper p_b curve, and thus the fibril

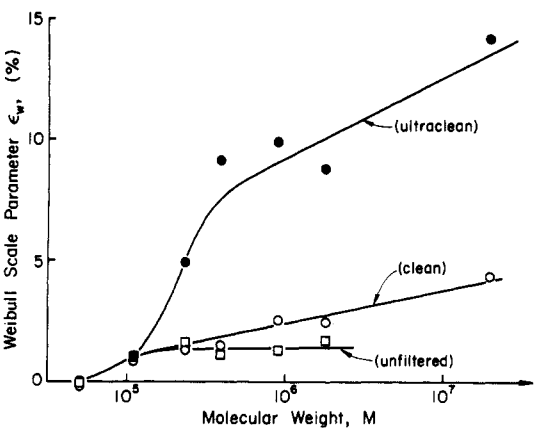

Figure 11. Weibull scale parameter ϵ_W vs. molecular weight in the various samples: unfiltered (□), "clean" (○), and "ultraclean" (●). Strain rate = 3 × 10^{-6} s^{-1}.

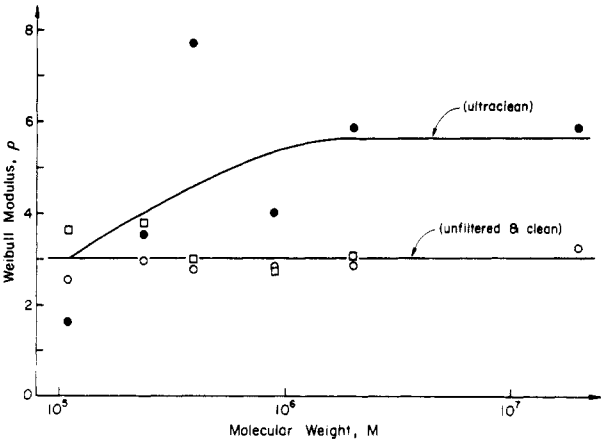

Figure 12. Weibull modulus ρ in the various samples: unfiltered (□), "clean" (○), and "ultraclean" (●). Strain rate = 3 × 10^{-6} s^{-1}.

breakdown events occur over a narrower region in strain. In the unfiltered specimens and the "clean" specimens ρ lies between 2.5 and 4, while for "ultraclean" specimens, ρ increases significantly, to about 5.5, in the high molecular weight samples which demonstrated high strains at failure. The values of ρ are shown in Figure 12. It will be suggested later that the variation of ρ with cleaniness is a result of the stress concentration associated with dust particle "seeds" coupled with an increasing drawing stress with plastic strain ϵ_p. The variation of the stress concentration around the irregular dust particles will naturally lead to a small value of ρ. For the "ultraclean" films where the breakdown is not dominated by the presence of dust, one suspects that the stress concentration at the intrinsic breakdown sites should be more uniform than that around dust particles. The net result is that ρ increases.

Physically the Weibull constants ρ and ϵ_W, unlike the median strain ϵ_b, are material constants. They should be independent of specimen geometry, for example. From eq 1, an increase in film square volume V_0 should lead to a reduction in median strain ϵ_b for breakdown. (This strain corresponds to breakdown at **p** = 0.5). This reduction can be predicted quantitatively by using the constants ρ and ϵ_W. To show that the predicted size effect exists, we recall the smaller copper grids, about 9 times smaller in area than the standard squares, which were used to prepare smaller film squares. The fibril stability of crazes in the smaller film square samples was investigated by using procedures identical with those used previously. The smaller film squares indeed showed a higher (extrapolated) ϵ_b, and the material constants ρ and ϵ_W determined from the data of

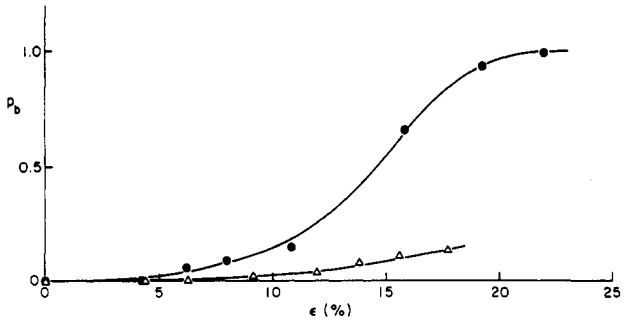

Figure 13. Breakdown probability p_b vs. strain for large and small film squares in the "clean" PS films (M = 1800). Large film square (●): ρ = 3.1, ϵ_W = 3.3%. Small film square (△): ρ = 3.4, ϵ_W = 4.1%.

the smaller samples were found to be the same as those for the larger film squares within experimental error (Figure 13). The size effect is well predicted by the change in V_0 in eq 1.

The size effect was verified by one more test. The fibril breakdown data for all the smaller film squares, a total of about 350 squares, were fed into a computer and randomly grouped into larger "squares", made up of a fixed number, N_g, of smaller squares. The median breakdown strains ϵ_b for the corresponding larger "squares" was then computed. As N_g increases, the curve of p_b vs. strain shifts toward smaller strains. Up to N_g = 64, the Weibull constants ρ and ϵ_W may be obtained from the Weibull plot. Within experimental error (which becomes larger due to statistical fluctuation at the largest N_g's) ρ and ϵ_W are independent of square size. The median breakdown strain for each random grouping of squares was determined by interpolation using the experimental Weibull distribution (ρ and ϵ_W) for that group (N_g). These ϵ_b's were then compared with ϵ_b', the median breakdown strain predicted from the Weibull distribution for the standard squares. The value ϵ_b' is given from eq 1 as

$$\epsilon_b' - \epsilon_c = \epsilon_W[(V_b/V_0) \ln 2/N_g]^{1/\rho} \quad (3)$$

where V_0 is now the initial volume of a smaller film square. Figure 14 shows that the ϵ_b from grouping is very close to the Weibull prediction ϵ_b'. The results clearly show that the size effect predicted by the Weibull distribution is observed. With the knowledge of the Weibull scale parameter ϵ_W and the Weibull modulus ρ we may predict the fibril breakdown strain that results from scaling up or down the sample size by several orders of magnitude.

Discussion

Since the active drawing zone of strain-softened polymer seems to be the site of all breakdown, let us assume that within this zone the polymer molecules have a limited time to disentangle or break before strain-hardening processes stop the active deformation and the structure of the glass relaxes toward one of lower fluidity. During that limited time if the critical condition for fibril breakdown does not occur, the fibrillation will continue and adjacent bulk polymer will be drawn into the fibrils. Suppose, however, that occasionally all chains going from the active zone to the fibrils either disentangle or break. The result is the start of fibril breakdown. Let us suppose, though we have little evidence to go on, that it is the disentanglement of the strands of the entanglement network, after the fibril surfaces have formed in the active zone, that is the critical step in fibril breakdown.

A PS chain of high molecular weight, say 800 000, is much longer than the entanglement spacing as reflected in M_e, the entanglement molecular weight ≈19 000 for PS).

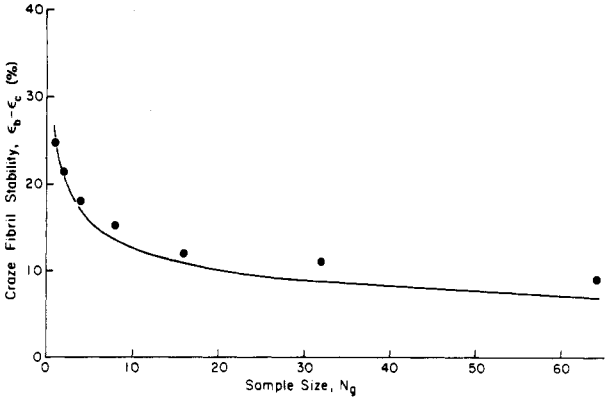

Figure 14. Comparison of the grouping data (●) with the prediction of the Weibull distribution (solid line). N_g = 1 corresponds to the volume of a small grid square, 4.4 × 10^{-14} m^3.

How can we rationalize the existence of an extremely fast and effective disentanglement process required for the complete discontinuity in fibrils? One possible and useful explanation comes from the suggestion that a significant entanglement loss is introduced during the fibrillation. In the active zone, the entanglement network of the polymer is forced to undergo chain scission by the shear stresses at the bulk–craze interface to accommodate the fibril drawing. Since the chains in the network have a Gaussian conformation, the scissions basically occur at random and reduce the number of entangled strands in the fibril from $n_0 \approx 50$ to a random number N_e of effectively entangled strands having mean $n_e \approx 30$, as will be demonstrated below. It is reasonable to assume furthermore that the scissions are statistically independent, requiring that N_e follow a binomial distribution with parameters n_0 and $q = n_e/n_0$, where q is actually the probability that a given strand does not undergo scission.

For a given effectively entangled strand in a fibril we let ξ be the probability that it disentangles in the active zone and treat disentanglements also as statistically independent. We let N_d be the number of the N_e which do not disentangle. Then to be one of the N_d strands an original entangled strand must neither undergo scission nor disentangle, and this probability is $q(1 - \xi)$. The n_e original strands are still statistically independent under this two-step process so that N_d also follows a binomial distribution, but with parameters n_e and $q(1 - \xi)$.

Next we postulate that a weak spot results if N_d is reduced to zero; i.e., all $N_e > 0$ disentangle (or $N_e = 0$). From the binomial distribution this probability is $[1 - q(1 - \xi)]^{n_0}$. Since $q(1 - \xi)$ is expected to be much less than one we have the accurate approximation

$$[1 - q(1 - \xi)]^{n_0} \approx \exp[-n_0 q(1 - \xi)] = \exp[-n_e(1 - \xi)] \quad (4)$$

Significant disentanglement (or post-fibril-formation scission) is necessary to create a weak spot. If ξ were zero then for a typical n_e of 30 the probability of weak spot formation is $\approx 10^{-13}$, the probability that $N_e = 0$ due to the initial scissions alone. This probability times the total number of entanglement tranfer lengths[4,14] in the craze fibrils in one film square ($\approx 10^{10}$ at ϵ_p = 0.1) is orders of magnitude less than one. Chain scission during fibril formation alone cannot account for the observed craze fibril breakdown.

Through the kinetic processes of disentanglement we expect ξ to be a complicated, increasing function $\xi(\sigma)$ of the drawing stress σ, which was postulated to increase as a power of ϵ_p (see Appendix 1). Using approximations given in detail in Appendix 1 it is possible to relate this form to the measured Weibull modulus ρ and derive the

following expression for the fibril stability ($\epsilon_b - \epsilon_c$):

$$\epsilon_b - \epsilon_c = \exp[n_e(1 - \xi(\sigma_0))/\rho]\{(\mathbf{n}_f V_0)^{-1}(\lambda - 1)\rho \ln 2\}^{1/\rho} \quad (5)$$

where $\mathbf{n}_f$ is the the number of fibril elements (total number of entanglement transfer lengths in the fibrils) formed from a unit risk volume V and $\xi(\sigma_0)$ is the strand disentanglement probability at the drawing stress σ_0 which corresponds to $\epsilon_p = 1$. The primary point of interest is the strong dependence of fibril stability on the parameter n_e, both explicitly in the exponential and implicitly through ρ. From binomial statistics one can show that the n_e dependence will still dominate if one chooses alternate criteria for a weak spot, e.g., $N_d \leq k$, where k is some small critical number satisfying $k \ll n_e$.

The quantity n_e can be calculated from the structural parameters of the craze fibril and the entanglement network and is given by[4,14]

$$n_e = qn_0 \quad (6)$$

where q is the survival probability of each entangled strand during fibrillation and n_0, the total number of entangled strands before fibrillation in the "phantom fibril" from which a craze fibril is drawn, is given by[4,14]

$$n_0 = \pi d\nu D_0^2(1 - M_e/M_n)/8 \quad (7)$$

where D_0 is the average craze fibril spacing, ν is the entanglement density calculated from the shear modulus $G_N°$ on the rubbery plateau to be 3.3×10^{25} m^{-3} for PS, M_e is the entanglement molecular weight computed from $G_N°$, and d is the end-to-end distance between adjacent entanglement points in the bulk. The factor $(1 - M_e/M_n)$ is the correction of ν for the finite chain length.[15] The average fibril spacing D_0 was measured by low-angle electron diffraction (LAED)[16] and Fourier transform image analysis[17] and was found to be around 20 nm in the freshly drawn craze microstructure. D_0 is a constant for PS for M's higher than 110 000 (at room temperature and strain rate = 3×10^{-6} s^{-1}). The mesh size of the entanglement network d is obtained from[18]

$$d = k(M_e)^{1/2} \quad (8)$$

to be 9.6 nm. To calculate the survival probability q, two approaches can be used. It can be calculated either from the method of geometrical statistics[14] or by using the Gaussian statistics of the random coil.[19] Both methods yield similar results, $q \approx 0.50$. The Weibull modulus ρ as a function of n_e is obtained from Figure 12 as described in Appendix 1. The value of $\mathbf{n}_f$ is approximately equal to $1/(dD_0^2) = 2.5 \times 10^{23}$ m^{-3} and $V_0 = 4 \times 10^{-13}$ m^3. From these values everything in eq 25 is known except $\xi(\sigma_0)$, which must lie between zero and one.

Figure 15 shows a plot of the fibril stability, $(\epsilon_b - \epsilon_c)$, vs. n_e for the "ultraclean" films. The solid lines correspond to the fibril stability computed from eq 5 for three different values of $\xi(\sigma_0)$, 0.45, 0.50, and 0.55. The best fit to the data (in a least-squares sense) is obtained with a disentanglement probability of 0.51. While $\xi(\sigma_0)$ is relatively insensitive to the initial molecular weight M, and thus n_e, the evidence in Figure 15 suggests that it increases somewhat as M decreases. The weak dependence of $\xi(\sigma_0)$ on M is not unexpected since although the final molecular weight of strands in the active zone will be severely decreased due to the chain scission necessary to form the fibril surfaces, some influence of the initial molecular weight on the final molecular weight will be retained.[14] The important point to be emphasized is that the fit of the theoretical curve to the data is quite satisfactory, especially considering the constraints on the single adjustable parameter, $\xi(\sigma_0)$.

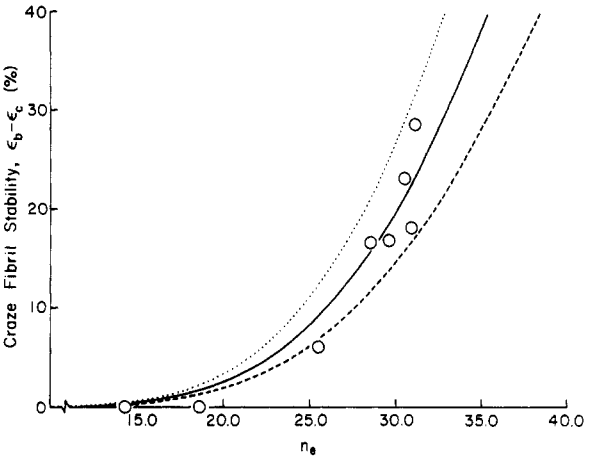

Figure 15. Plot of fibril stability ($\epsilon_b - \epsilon_c$) vs. n_e, the average effective number of entangled strands per fibril after fibrillation for the "ultraclean" specimens. The lines give the theoretical curves for disentanglement probability $\xi(\sigma_0)$: (···) 0.45; (—) 0.50; (– – –) 0.55.

The local stress undoubtedly plays an important role in fibril breakdown. Dust particle inclusions in the unfiltered specimens give rise to stress concentrations, which speed up the disentanglement processes and lead to much earlier fibril breakdown in comparison to the "clean" or "ultraclean" specimens. Although the average stress concentration of the inclusions is insensitive to the inclusion size, the stress decays more slowly with distance from the inclusion for larger inclusions. However, a larger risk volume is associated with a larger inclusion, which may also lead to the observed particle size effects on the fibril breakdown behavior as well as lower values of ρ due to the increased variability associated with variable particle size. An increase in strain rate, which will result in a higher drawing stress on the PS film, should reduce the fibril stability as observed.

Because all the inherent weak spots or dust particles are distributed at random throughout the initial volume, one would expect the hazard rate of encountering one of these to be constant with the plastic strain ϵ_p as the risk volume increases. Assuming that the weak spots are time independent and that the drawing stress is constant on the bulk–craze interface, the plastic strain at fibril breakdown ought to follow the exponential distribution, i.e., a Weibull distribution, eq 1, with Weibull modulus $\rho = 1$. But values of ρ much greater than one are consistently observed for the film squares, and this observation strongly suggests that in these experiments the drawing stress σ increases with plastic strain ϵ_p as postulated in our derivation of eq 1 in Appendix 1.

Nevertheless, the higher than unity Weibull modulus ρ for the dust-containing films could be due to debonding of the particles in the glass as a function of time before they are drawn to the craze interface. Such debonding would result in an increasing hazard rate of breakdown at larger times and larger strains. To check whether a time-dependent debonding actually exists, a simple test was performed. Starting at the same time two identical specimens were strained to measure the fibril stability. The control specimen was strained to complete fracture as usual, which took about 18 h. The other specimen was interrupted during the test at the point when fibril breakdown was starting to occur. The test was then resumed after a delay of 1 week. If time-dependent debonding of dust particles exists, logically the breakdown data of the interrupted specimen would show a break in

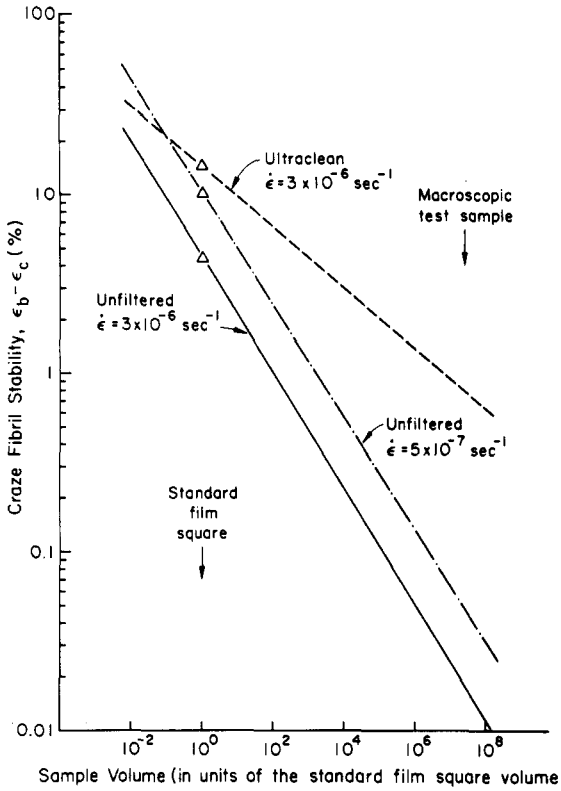

Figure 16. Median plastic strain ($\epsilon_b - \epsilon_c$) predicted from Weibull statistics to produce one craze fibril breakdown in a volume V for PS of $M = 1\,800\,000$. Volumes of a standard film square and a macroscopic test sample are marked.

the Weibull plot at the strain of interruption. However, the delay produced no change in the Weibull plots. We thus believe that the stress on the film increases as strain is increasing, so that the term $(\epsilon_p/\epsilon_W)^\rho$ in eq 1 actually represents primarily the stress dependence of the fibril failure process through eq 11 of Appendix 1.

The craze fibril breakdowns observed here take place at very low strain rates, much lower than the rates of impact testing often used to characterize the fracture of polymer glasses. However, the low strain rates allow us to simplify the complicated fracture process and allow us to concentrate on the study of craze breakdown, especially that in the early stage of polymer failure. The "pear-drop-shaped" cavities we observe at the craze interface are consistent with the morphology of features observed on the bulk fracture surfaces in the region corresponding to the initial slow crack growth.[5,20] The data presented here thus provide one more piece of evidence for the assertion that the fracture of unprecracked glassy polymers is controlled by breakdown of crazes to form cracks. The information brought out by the fibril breakdown statistics may be useful in controlling the onset of crack growth. Figure 16 is a graph showing the median value of ϵ_b for fibril breakdown vs. sample size predicted from the constants ϵ_W and ρ for the standard film squares using the Weibull distribution. The statistical data obtained from the film squares can be used to predict the behavior of typical polymer tensile samples, which are several orders of magnitude larger in scale than our films.

Certainly the strong increase in craze fibril stability in the range of molecular weight 50 000–200 000 is mirrored by an equally strong increase in the fracture stress of smooth specimens.[21-23] It points to the fact that to produce tougher polymer glasses we must control the breakdown of the craze fibrils. We could try to prevent crazes from forming in the first place, e.g., by electron irradiation cross-linking[24] or blending with other, higher entanglement density polymers,[18,25,26] causing the polymer to deform preferentially by shear. On the other hand, we could decrease the average stresses on the crazes, e.g., by rubber modification or by decreasing the hard-particle inclusion content to delay fibril breakdown. A combination of both strategies may be the most effective way to toughen polymer glasses.

Conclusions

(1) A simple test has been developed to investigate quantitatively craze fibril stability and the fibril breakdown statistics in thin polymer films.

(2) A large increase in craze fibril stability with increasing molecular weight M was found in the same region, from 50 000 to 200 000, as the increase in the fracture stress of macroscopic specimens. Above 200 000 the fibril stability increases much more slowly with M.

(3) Dust particle inclusions strongly suppress craze fibril stability. However, they can be removed by preparing specimens in clean environments.

(4) For PS, craze fibril breakdown always occurs at the craze–bulk interface.

(5) Increasing the strain rate reduces the craze fibril stability by increasing the drawing stress under which the fibrils are created at the craze–bulk interface.

(6) Craze fibril breakdown statistics follow a Weibull distribution in strain. The Weibull modulus ρ and scale parameter ϵ_W can be used to scale the results from small-scale films to large specimens.

(7) The molecular weight dependence of craze fibril stability can be successfully rationalized by a statistical model in which the critical event is the disentanglement of the n_e remaining entangled molecular strands in a fibril within the active zone at the craze–matrix interface. The probability of disentanglement of any single strand is approximately 0.5.

Acknowledgment. We gratefully acknowledge primary financial support by the Cornell Materials Science Center for E.J.K., C.C.K., and S.L.P. as well as the use of the facilities of the Cornell Materials Science Center, which is funded by the NSF DMR-MRL program. A.C.-M.Y. was supported by a grant from the U.S. Army Research Office Durham, NC. We also appreciate the use of the clean room facilities of NRRFSS for producing the "ultraclean" films.

Appendix 1

Weibull Breakdown Statistics. The fibril breakdown strain for a given film square was defined as the strain at which a void first appeared within a craze in that square. This breakdown strain was treated as a random variable, with distribution function $p_b(\epsilon)$. The sources of randomness were scattered dust particles and intrinsic weak spots, which we now attempt to relate to $p_b(\epsilon)$. Consider a single film square with an initial volume V_0. As the strain is increased a craze is initiated at a certain strain ϵ_c, which we take to be deterministic. Further increases in the strain ϵ generate a risk volume V, which is the total volume of the original polymer film square converted to craze fibrils. It may be shown that

$$V = V_0\epsilon_p/(\lambda - 1) \tag{9}$$

where V_0 is the initial film square volume, λ is the craze fibril extension ratio, and ϵ_p is the plastic strain, $(\epsilon - \epsilon_c)$.

Next imagine that "seeds" for craze fibril breakdown, dust particles and weak spots, exist randomly scattered throughout the volume V. It is natural to view these as

occurring as a compound Poisson process in space,[27] the compound feature arising from the varying severity of the seeds. As the plastic strain ϵ_p increases, the craze expands by the advancement of the craze–bulk interface into the bulk. For a small change in plastic strain $d\epsilon_p$ the change in risk volume dV, within which a seed may be encountered, is from eq 9

$$dV = V_0(\lambda - 1)^{-1}\, d\epsilon_p \tag{10}$$

It has been observed that craze fibril breakdown in PS always occurs at the craze–bulk interface instead of at the midrib, the oldest region of the fibril structure. Therefore it is not possible to attribute fibril breakdown to creep since this would cause a progressive failure of existing fibrils. On the contrary, it appears that the molecular process of fibril breakdown will not start until a sufficiently severe random "seed" is encountered at the craze–bulk interface. This observation implicates the "active drawing zone", a thin (<10 nm) layer of strain-softened material in the bulk polymer adjacent to the craze which is in the process of being drawn into craze fibrils.

Next postulate that the stress (the drawing stress) in the fibrils forming adjacent to the active drawing zone increases as a power of the plastic strain ϵ_p; i.e.

$$\sigma = \sigma_0(\epsilon_p)^\gamma, \qquad \epsilon_p \geq 0 \tag{11}$$

where $\sigma_0 > 0$ and $\gamma \geq 0$ are constants. This formulation admits to the important cause $\gamma = 0$ whereby the drawing stress σ becomes the constant σ_0 for all $\epsilon_p > 0$. Now when a seed enters the active drawing zone it may initiate fibril breakdown if it is sufficiently severe relative to the drawing stress σ. Accordingly we let $\Lambda(\sigma)$ be the mean number of seeds per unit volume of bulk which, when encountered by the craze–bulk interface, will initiate fibril breakdown in the active drawing zone. Furthermore, we assume that $\Lambda(\sigma)$ is given by a power law in the drawing stress, viz.

$$\Lambda(\sigma) = (\sigma/\sigma_b)^\delta/V_b, \qquad \sigma \geq 0 \tag{12}$$

where V_b, σ_b, and δ are positive constants. (V_b is the volume in which one breakdown seed will be encountered at a stress σ_b. In what follows σ_b will be chosen so that V_b equals the volume of one large film square, 4×10^{-13} m^3.) Thus $\Lambda(\sigma)$ plays the role of the intensity in the compound Poisson process.[27]

Under the plastic strain σ_p we let $\mathbf{p}(\epsilon_p)$ be the probability that fibril breakdown has occurred somewhere in the film square. Using arguments appropriate to the compound Poisson process,[27] one may show that

$$\mathbf{p}(\epsilon_p) = 1 - \exp\left[-\int_0^{\epsilon_p} \Lambda(\sigma_0\epsilon^\gamma)\, dV(\epsilon)\right] \tag{13}$$

where ϵ is a dummy strain variable of integration. Essentially the integral in eq 13 represents the cumulative hazard as the plastic strain is increased from zero to ϵ_p. using eq 10–12 explicitly one finds that eq 13 becomes

$$\mathbf{p}(\epsilon_p) = 1 - \exp\{-(\sigma_0/\sigma_b)^\delta(V_0/(V_b(\lambda - 1)))[(\epsilon_p)^{\gamma\delta+1}/(\gamma\delta + 1)]\} \tag{14}$$

This is a Weibull distribution function, which may be rewritten for convenience as

$$\mathbf{p}(\epsilon_p) = 1 - \exp[-(V_0/V_b)(\epsilon_p/\epsilon_W)^\rho] \tag{15}$$

where $\rho = \gamma\delta + 1$ is the Weibull modulus or shape parameter and

$$\epsilon_W = [(\sigma_b/\sigma_0)^\delta(\lambda - 1)(\gamma\delta + 1)]^{1/(\gamma\delta+1)} \tag{16}$$

is the Weibull scale parameter relative to $V_0 = V_b$ in the event that $\gamma = 0$, i.e., the drawing stress is σ_0 independent of plastic strain, $\rho = 1$ and eq 16 simplifies to

$$\epsilon_W = (\sigma_b/\sigma_0)^\delta(\lambda - 1) \tag{17}$$

Disentanglement Probability ξ and the Weibull Modulus ρ. Since it is not possible at this stage to calculate $\exp[-(1 - \xi)]$ vs. ϵ_p directly, we make the power law approximation

$$\exp[-(1 - \xi(\sigma))] \approx (\sigma/\sigma_f)^h \tag{18}$$

valid over the limited range of σ where fibril drawing and breakdown occur and where σ_f and h are positive constants.

Next let $\mathbf{n}_f$ be the number of fibril elements (total number of entanglement transfer lengths in the fibrils) formed from a unit risk volume V. Through the connection of the compound Poisson process for weak spots and weakest-link statistics (assuming fibril breakdowns are statistically independent) we may show the correspondence

$$\Lambda(\sigma) = (\sigma/\sigma_b)^\delta/V_b = \mathbf{n}_f(\sigma/\sigma_f)^{n_e h} \tag{19}$$

where the middle term comes from eq 12 and the last term is its present equivalent, being approximately the number of fibril breakdowns per unit risk volume which will occur in the active zone under stress σ. Thus the connection is

$$\delta = n_e h \tag{20}$$

and

$$\sigma_b = \sigma_f(\mathbf{n}_f V_b)^{-1/(n_e h)} \tag{21}$$

The Weibull modulus is given by

$$\rho = \gamma\delta + 1 = (\gamma h)n_e + 1 \tag{22}$$

The Weibull modulus ρ as a function of n_e is obtained from a least-squares fit of eq 22 to the data in Figure 12; γh is determined to be 0.13 for the ultraclean samples.

Using eq 15, 16, 18, 20, and 21 one can express the fibril stability in terms of n_e as follows:

$$\epsilon_b - \epsilon_c = \exp[n_e(1 - \xi(\sigma_0))/\rho]\{(\mathbf{n}_f V_0)^{-1}(\lambda - 1)\rho \ln 2\}^{1/\rho} \tag{23}$$

where $\xi(\sigma_0)$ is the strand disentanglement probability at the drawing stress σ_0 which corresponds to $\epsilon_p = 1$.

Appendix 2. List of Symbols

K, α	Mark–Houwink parameters
h	exponent in the disentanglement power law, $\exp[-(1 - \xi(\sigma))] \cong (\sigma/\sigma_f)^h$
M, M_v	molecular weight and viscosity-average molecular weight
M_e	entanglement molecular weight from $G_N°$, the shear modulus on the rubbery plateau
N_d	random number of strands in fibril that do not disentangle
N_e, n_e	random number and mean number, respectively, of effectively entangled strands in fibril surviving fibril surface formation
N_g	number of small film squares randomly grouped to form larger grid "square"
N_0	number of independent film squares in grid
n_0	initial number of entangled strands in fibril before strands are broken to form fibril surfaces
$\mathbf{n}_f$	number of fibril elements (entanglement transfer lengths) formed from unit risk volume V

p_b cumulative number fraction of film squares which have undergone local craze fibril breakdown

p_c cumulative number fraction of film squares which have undergone craze initiation

p_f cumulative number fraction of film squares which have undergone catastrophic fracture

$\mathbf{p}(\epsilon_p)$ probability that fibril breakdown has occurred somewhere in film square at a plastic strain ϵ_p

q probability (n_0/n_e) of entangled strand survival

V risk volume, the volume of the film square converted into craze fibrils

V_b volume in which one breakdown seed is encountered at stress σ_b

V_0 initial volume of grid square

γ exponent in the power law for crazing stress, $\sigma = \sigma_0(\epsilon_p)^\gamma$

δ exponent in the power law for seed density, $\Lambda(\sigma) = (\sigma/\sigma_b)^\delta/V_b$

ϵ nominal tensile strain applied to film squares

ϵ_b, ϵ_c, ϵ_f median strain for craze breakdown, initiation, and catastrophic fracture, respectively

ϵ_b' median breakdown strain predicted from the Weibull distribution

ϵ_p plastic strain = $(\epsilon - \epsilon_c)$

ϵ_W Weibull scale parameter

λ craze fibril extension ratio

$\Lambda(\sigma)$ seed density, the mean number of "seeds" per unit volume of bulk polymer that will initiate breakdown at a crazing stress σ

η_{sp}, $[\eta]$ specific viscosity and intrinsic viscosity, respectively

ρ Weibull modulus

σ crazing (drawing) stress

σ_f parameter in the disentanglement power law, $\exp[-(1 - \xi(\sigma))] \cong (\sigma/\sigma_f)^h$

σ_0 parameter in the power law for crazing stress, $\sigma = \sigma_0(\epsilon_p)^\gamma$

σ_b parameter in the power law for seed density, $\Lambda(\sigma) = (\sigma/\sigma_b)^\delta/V_b$

$\xi(\sigma)$ probability of strand disentanglement in active zone at craze–bulk interface at stress σ

Registry No. PS (homopolymer), 9003-53-6.

References and Notes

(1) Rabinowitz, S.; Beardmore, P. *CRC Rev. Macromol. Sci.* **1972**, *1*, 1.
(2) Kambour, R. P. *J. Polym. Sci., Part D* **1973**, *7*, 1.
(3) Gent, A N. *AMD* [*Symp. Ser.*] *Am. Soc. Mech. Eng.* **1976**, *19*, 55.
(4) Kramer, E. J. *Adv. Polym. Sci.* **1983**, *52/53*, 1.
(5) Beahan, P.; Bevis, M.; Hull, D. *Proc. R. Soc. London, Ser. A* **1975**, *343*, 525.
(6) Doyle, M. J.; Maranci, A.; Orowan, E.; Stork, S. T. *Proc. R. Soc. London, Ser. A* **1972**, *329*, 137.
(7) Lauterwasser, B. D.; Kramer, E. J. *Philos. Mag.* **1979**, *A39*, 469.
(8) Verheulpen-Heymans, N. *Polym. Eng. Sci.* **1984**, *24*, 809.
(9) Trassaert, P.; Schirrer, R. *J. Mater. Sci.* **1983**, *18*, 3004.
(10) Schirrer, R.; Le Masson, J.; Tomatis, B. *Polym. Eng. Sci.* **1984**, *24*, 820.
(11) Lauterwasser, B. D. Ph.D. Thesis, Cornell University, Ithaca, NY, 1979.
(12) Weibull, W. *J. App. Mech.* **1951**, *18*, 293.
(13) Glandus, J. C.; Boch, P. *J. Mater. Sci. Lett.* **1984**, *3*, 74.
(14) Kramer, E. J. *Polym. Eng. Sci.* **1984**, *24*, 761.
(15) In making this chain-end correction we have assumed that two initial chain ends have the same effect as one chain scission during fibril formation. Since we assume that each scission removes one, and only one, strand from the network, the correction factor is $(1 - M_e/M_n)$, rather than the usual $(1 - 2M_c/M_n)$ for a randomly cross-linked network (Flory, P. J. *Principles of Polymer Chemistry*; Cornell University: Ithaca, NY, 1953).
(16) Yang, A. C.-M.; Kramer, E. J. *J. Polym. Sci., Polym. Phys. Ed.* **1985**, *23*, 1353.
(17) Yang, A. C.-M.; Kramer, E. J. *J. Mater. Sci.*, to be published.
(18) Donald, A. M.; Kramer, E. J. *Polymer* **1982**, *23*, 461.
(19) Kuo, C. C.; Phoenix, S. L.; Kramer, E. J. *J. Mater. Sci. Lett.* **1985**, *4*, 459.
(20) Hull, D. *J. Mater. Sci.* **1970**, *5*, 357.
(21) Fellers, J. F.; Kee, B. F. *J. Appl. Polym. Sci.* **1974**, *18*, 2355.
(22) McCormick, H. W.; Brower, F. M.; Kin, L. *J. Polym. Sci.* **1959** *39*, 87.
(23) Vincent, P. I. *Polymer* **1960**, *1*, 425.
(24) Henkee, C. S.; Kramer, E. J. *J. Polym. Sci., Polym. Phys. Ed.* **1984**, *22*, 721.
(25) Berger, L. B.; Kramer, E. J., unpublished.
(26) Donald, A. M.; Kramer, E. J. *J. Mater. Sci.* **1982**, *17*, 1871.
(27) Karlin, S.; Taylor, H. M. *A Second Course in Stochastic Processes*, 1st ed.; Academic: New York, 1982; pp 426–441.